Trim Investigation for Coaxial Rigid Rotor Helicopters Using an Improved Aerodynamic Interference Model

Ye Yuan, Renliang Chen, Pan Li*

National Key Laboratory of Rotorcraft Aeromechanics, Nanjing University of Aeronautics & Astronautics, Nanjing, China

Abstract

The coaxial rigid rotor helicopter has been proposed as a future high-performance rotorcraft concept. However, the aerodynamic interference of this helicopter is complicated because it couples with the unique flapping feature of the rigid rotor, which further alters the trim characteristics of coaxial rigid rotor helicopters. Thus, a multi-point vortex ring element (MVRE) model is developed to simulate the aerodynamic interference between rotors. The method for establishing this MVRE model is illustrated, and a wind tunnel experimental dataset is used to assess its precision in both hover and forward flight states. Next, a flight dynamics model of the coaxial rigid rotor helicopter is built based on the MVRE aerodynamic interference model and the flapping feature of the rigid rotor. The influence of the rotor wake on the fuselage and the horizontal and vertical tails can be also calculated by this model. The trim characteristics of this helicopter are evaluated with flight test data for speeds ranging from 0 m/s to 80 m/s, and the results affirm that this model can reflect the trim characteristics with satisfactory precision. In addition, the calculation process demonstrates that the MVRE model provides a much faster computing rate. Considering the aerodynamic interference and rigid rotor characteristics, the trim results of the coaxial rigid rotor helicopter presents unique features: aerodynamic interference in the coaxial rotor system not only could increase the collective pitch and the collective differential, but also adds a negative gradient under the forward speed in the longitudinal cyclic pitch in the low-speed forward flight range. Moreover, the rotor wake effect on the other parts of helicopter is distinct from the corresponding effects on conventional helicopters in terms of the trim characteristics.

Keywords: Coaxial Helicopter; Rigid Rotor; Aerodynamic Interference; Flight Dynamics Characteristics; Trim Characteristics

0. Nomenclature

C_T	Lift coefficient	R	Rotor radius (m)
K_β	Equivalent flapping spring rigidity (N.m/rad)	$\boldsymbol{R}_i$	State vector of the vortex ring motion
		X, Y, Z	External forces about the body axes (N)
I_β	Blade moment of inertia (kg.m^3)	$\bar{e}$	Non-dimensional flapping offset
L, M, N	External moments about the body axes (N.m)	m_k	Torque coefficient
		r_c	Vortex core radius (m)
M_{SUM}	Gross weight (kg)	Δt	Time step (s)
M_β	Blade mass static moment (kg.m^2)	$\boldsymbol{v}_f$	Velocity vector on the fuselage (m/s)
N_b	Number of blades	$\boldsymbol{v}_t$	Velocity vector on the tails (m/s)
V_f	Forward speed (m/s)	$\boldsymbol{v}_\infty$	Freestream velocity vector (m/s)

*Corresponding author. Tel.: +86 25 84892141
E-mail address: crlae@nuaa.edu.cn

Γ_c	Control phase angle (°)
Ω	Rotor Speed (rad/s)
β	Flapping angle (rad)
γ_c	Lock number
μ	Advancing ratio
θ, ϕ	Pitching and rolling attitude (°)
ρ	Air density (kg/m^3)
$\bar{\omega}_n$	Non-dimensional flapping frequency
ψ	Azimuth angle (°)

Subscripts

L	Lower rotor
U	Upper rotor
T	Tails
F	Fuselage

1. Introduction

The coaxial rigid rotor helicopter has attracted considerable research interest in recent years because of its high-speed performance [1] and outstanding cruise-efficiency [2]. Because of the reduced flapping amplitude of this rigid rotor system, the distance between upper and lower rotor centres may be far less than that of conventional helicopters to reduce the power consumption of the rotor hub [3]. However, the decrease in the rotor centre distance results in significant changes in the aerodynamic interference phenomenon, which in turn alters the trim features and other flight dynamics characteristics [4~7]. Moreover, the effects of the rotor wake on the fuselage and the horizontal and vertical tails should also be considered during the trim investigation.

In the flight dynamics modelling and trim investigation, the simulation method of aerodynamic interference must take both efficiency and accuracy into account. Researchers have utilized different types of inflow models based on momentum theory to investigate the aerodynamic interference of the coaxial helicopter [8~12]. These methods assume that the rotor inflow is linear, but in reality, the rotor inflow has many non-linear components, which influence the flapping motion and consequently change the hub moment of the rotor. Moreover, the aerodynamic interference between rotors further complicates the inflow characteristics. Thus, momentum theory methods cannot have sufficient accuracy in the inflow calculation of the coaxial rotor. Furthermore, methods based on momentum theory present difficulty in simulating the rotor wake effect on the horizontal tail and the other parts of helicopters. In addition, although the CFD (computational fluid dynamics) [13~15] and VPM (viscous vortex particle method) [16, 17] can be used to simulate the various types of aerodynamic interference with satisfactory precision, these methods are excessively time consuming and not suitable for flight dynamics analysis. Therefore, the development of a method to simulate the aerodynamic interference that is suitable for the trim and flight dynamics investigation of coaxial rigid rotor helicopters is in urgent demand. The free-wake method is widely used in the flight dynamics investigation, including that for coaxial helicopters [18~21]. However, although this method has an acceptable precision and the computing time is less than that of the CFD and VPM methods, this method still requires exorbitant computing time to achieve the trim state. On the other hand, Basset [22~24] performed research on the aerodynamic interference between the rotor and tail rotor in the conventional single-rotor helicopter and established a vortex ring element (VRE) model to analyse the effect of the aerodynamic interference between rotor and horizontal tails on the flight dynamics features. Although the VRE wake model ignores the wake dynamic extend-retract behaviour and cannot precisely simulate the aerodynamic interference phenomenon of the coaxial rigid rotor helicopters, the use of the proposed VRE model represents a potential method of simulating the aerodynamic interference of coaxial rigid rotor helicopters.

On the one hand, the aerodynamic interference would change the inflow of the coaxial rotor, which

influences the rotor aerodynamics and hub moment. On the other hand, the coaxial rigid rotor helicopter has distinct flight dynamics characteristics because of the higher flapping frequency [25]. The hub moment is highly dependent on this frequency; thus, the hub moment induced by the aerodynamic interference is much greater for the coaxial rigid rotor helicopter than for other types of helicopters, leading to additional changes in the trim characteristics. In addition, the flapping response lag angle is also a function of the flapping frequency [26]. This angle determines the azimuth angle of the hub moment. Therefore, the direction of the interference-induced hub moment is also different from that of the conventional coaxial helicopter, which further alters the flight dynamics characteristics of the coaxial rigid rotor helicopter.

In light of the proceeding discussion, the basic theory and modelling method of the multi-points vortex ring element (MVRE) model with the consideration of the rotor wake extend and retract behaviour is illustrated in this paper. The precision of the MVRE aerodynamic interference model is evaluated by comparison against wind tunnel experimental data in both hover and forward flight state. Next, the MVRE aerodynamic interference model is utilized to construct a flight dynamics model of the coaxial rigid rotor helicopter. Moreover, the effects of the rotor wake on the fuselage, horizontal and vertical tails are also calculated using the MVRE model. The accuracy of this flight dynamics model is assessed against the flight test data of the XH-59A helicopter. In addition, the proposed model is utilized to investigate the impacts of different types of aerodynamic interference on the trim characteristics of the coaxial rigid rotor helicopter.

2. MVRE Model

2.1 Physical Model

The MVRE model proposed in this article is based on Basset's research results [22~24]. The model is constructed on the basis of the rotor disc hypothesis and the classical fixed wake model. The model allows the consideration of the rotor wake's various distortion effects; therefore, it can be used to accurately simulate the wake geometry. The simplification process is shown in Fig. 1

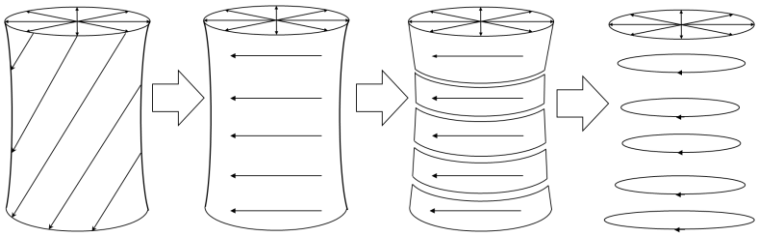

Fig. 1 Simplification process of the MVRE model

The vertical component of the cylindrical vortex has little effect on the induced velocity of the rotor, and the horizontal component is considered in the MVRE model. Thus, the wake is discretized as a number of vortex bands, with lengths given by $l_1, l_2, ...l_n$. When the vortex strength density is γ_i, the vorticity of the *i* th vortex band can be expressed as $\Gamma_i = \gamma_i l_i$. The vortex bands can be simplified as concentrated vortex rings, which is indicated in Fig. 1. When the length of the vortex band is sufficiently small, this simplification can be used to simulate the rotor wake and its effect on the helicopters.

2.2 Vortex Ring Kinematic Model

The vortex ring has 7 degrees of freedom: three position degrees of freedom (x_i, y_i, z_i), three angular degrees of freedom $(\theta_i, \varphi_i, \psi_i)$ and a radius extend-retract degree of freedom (r_i). The state vector of the vortex ring motion can be written as $\boldsymbol{R}_i = [x_i, y_i, z_i, \theta_i, \varphi_i, \psi_i, r_i]$, and the rotor wake can be expressed as $\boldsymbol{R} = [\boldsymbol{R}_1, \boldsymbol{R}_2, ..., \boldsymbol{R}_N]$, where *N* is the number of the vortex ring of the rotor wake. Therefore,

the equation of the vortex ring motion is obtained as follows:

$$\frac{d\boldsymbol{R}_i}{dt} = \boldsymbol{u}_i(\boldsymbol{R}) + \boldsymbol{v}_i(\boldsymbol{u}_h, \boldsymbol{R}_i) \tag{1}$$

where $\boldsymbol{u}_i$=[v_{xi},v_{yi},v_{zi},$\dot{\theta}_i$,$\dot{\phi}_i$,$\dot{\psi}_i$,$\dot{r}_i$] is the velocity vector of the vortex ring and can be obtained by the Biot-Savart law; $\boldsymbol{v}_i(\boldsymbol{u}_h, \boldsymbol{R}_i)$ is the relative velocity between the rotor and vortex ring; and $\boldsymbol{u}_h$ is the velocity vector of the rotor hub motion. $\boldsymbol{v}_i(\boldsymbol{u}_h, \boldsymbol{R}_i)$ can be easily obtained through the flight dynamics model and the transformation of the coordinates.

Because the vortex ring in the MVRE model is simplified from the vortex bands, the length of the vortex bands and its vorticity can be written as follows:

$$l_i = \Delta t(v_0 + w_h) \tag{2}$$

$$\Gamma_i = \Delta t\gamma(v_0 + w_h) \tag{3}$$

where v_0 is the induce velocity on the rotor; w_h represents the vertical velocity at the rotor hub. The vortex strength density γ is a function of the azimuth angle and given as follows:

$$\gamma = \gamma_0 + \gamma_{1c}\cos(\psi) + \gamma_{1s}\sin(\psi) \tag{4}$$

where γ_0, γ_{1c}, and γ_{1s} can be determined by the lift, pitching and rolling aerodynamic moment coefficients of rotor (C_T, C_L, C_M), respectively [27].

To calculate $\boldsymbol{u}_i(\boldsymbol{R})$, the j th vortex ring in the wake is discretized as a number of calculation points $P_{i,j}$ (vortex segment) with the same azimuth angle distance as illustrated in Fig. 2, the vorticity of which is obtained using Eqns. (3~4) and can be represented as $\Gamma_{i,j}$. Thus, the Biot-Savart law can be used to calculate its induced velocity at any point in space, and the vortex ring-induced velocity at point q is obtained by integration of every calculation point. Therefore, the wake-induced velocity is determined by further integrating the induced velocity of every vortex ring, which is:

$$v_q = \sum_{j=1,N}\sum_{i=1,M} \boldsymbol{f}(p_{i,j}, \Gamma_{p_{i,j}}, q) \tag{5}$$

where $\boldsymbol{f}$ is the induced velocity calculation method according to the Biot-Savart law, and M is the number of calculation points in every vortex ring. Eq. (5) can be used to calculate the induced velocity on the rotor and the wake induced velocity on the fuselage and tails.

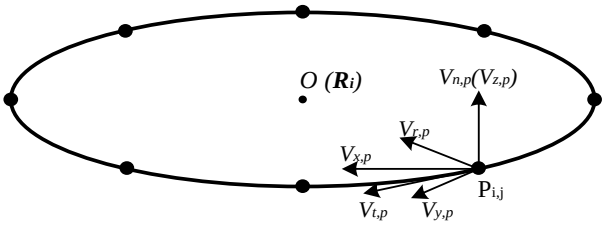

Fig. 2 Calculation point on the vortex ring

However, calculating the velocity induced by the same vortex ring or when the vortex ring that is close to the calculation point is a more complex process because the distance may lead to inaccuracy. Thus, Vatistas' correction [28,29] is utilized in this aerodynamic interference model. The schematic diagram of this vortex segment calculation method is shown in Fig. 3.

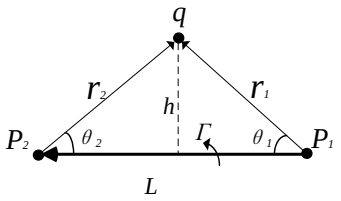

Fig. 3 Schematic diagram of the vortex segment calculation

Vatistas' correction was developed based on Biot-Savart law along with the concept of the viscous core radius to improve the precision. The velocity at point q induced by vortex segment P_1P_2 is calculated as follows:

$$\boldsymbol{v}_{q,P_1P_2} = \frac{\Gamma_{P1P2}}{4\pi} \frac{h}{\sqrt[n]{r_c^{2n} + h^{2n}}} (\cos\theta_1 - \cos\theta_2)\boldsymbol{i} \tag{6}$$

where h is the vertical distance between the point and the vortex segment; n represents the vortex core model parameter, and $\boldsymbol{i}$ is the reference vector.

Eqns. (5~6) can be utilized to obtain the wake-induced velocity on the calculation point of the vortex ring, which is used to determine $\boldsymbol{u}_i(\boldsymbol{R})$ in Eq. (1). The velocity vector at each calculation point in both earth coordinates $V_{x,p}, V_{y,p}, V_{z,p}$ and the local coordinates $V_{t,p}, V_{r,p}, V_{n,p}$ in Fig.2 are also imposed in this process:

1) The translational velocities of the vortex ring, v_{xi}, v_{yi}, v_{zi}, are determined by the average velocities $V_{x,p}, V_{y,p}, V_{z,p}$ of every calculation point.
2) The pitching and rolling angular velocities, $\dot{\theta}_i, \dot{\varphi}_i$, are determined by the least square approximation based on the normal velocity $V_{n,p}$ at every calculation point.
3) The yawing angular velocity $\dot{\psi}_i$ and extend-retract velocity $\dot{r}_i$ are calculated by the average values of $V_{t,p} / r_i$ and $V_{r,p}$ respectively.

Therefore, the equation of the vortex ring motion and description of the MVRE model are illustrated, in which the rotor wake motion equation and the wake-induced velocity calculation process can be obtained.

The geometry of the vortex ring changes at every time step, which would lead to additional alteration of the induced velocity on the rotor. This alteration would influence the vortex strength density and further affect the wake geometry. Thus, during the trim process, the vortex ring model keeps calculating until the rotor aerodynamic characteristics reach the convergence condition.

2.3 Application to Coaxial Rotor

The aerodynamic interference between the coaxial rotors can be divided into two aspects: the aerodynamic interference between wakes and the wake effect of one rotor on the inflow of the other rotor.

Based on the aerodynamic feature of the coaxial rotor, the motion equation of the coaxial rotor wake in MVRE model can be rewritten as:

$$\begin{aligned} \frac{d\boldsymbol{R}_{i,L}}{dt} &= \boldsymbol{u}_i(\boldsymbol{R}_L) + \boldsymbol{u}_i(\boldsymbol{R}_U) + \boldsymbol{v}_i(\boldsymbol{u}_h, \boldsymbol{R}_{L,i}) \\ \frac{d\boldsymbol{R}_{i,U}}{dt} &= \boldsymbol{u}_i(\boldsymbol{R}_U) + \boldsymbol{u}_i(\boldsymbol{R}_L) + \boldsymbol{v}_i(\boldsymbol{u}_h, \boldsymbol{R}_{U,i}) \end{aligned} \tag{7}$$

The second term in Eq. (7) donates the aerodynamic interference between the wakes of the coaxial rotor. Moreover, to simulate the wake effect of one rotor on the inflow of the other rotor, the wake-induced

velocities on the upper and lower rotors are rewritten from Eq. (5) as follows:

$$\begin{aligned} v_{q,L} &= \sum_{j=1,N}\sum_{i=1,M} \boldsymbol{f}(p_{i,j,L},\Gamma_{p_{i,j},L},q_L)+\sum_{j=1,N}\sum_{i=1,M} \boldsymbol{f}(p_{i,j,U},\Gamma_{p_{i,j},U},q_L) \\ v_{q,U} &= \sum_{j=1,N}\sum_{i=1,M} \boldsymbol{f}(p_{i,j,U},\Gamma_{p_{i,j},U},q_U)+\sum_{j=1,N}\sum_{i=1,M} \boldsymbol{f}(p_{i,j,L},\Gamma_{p_{i,j},L},q_U) \end{aligned} \tag{8}$$

where $v_{q,L}$ and $v_{q,U}$ are the induced velocities at points on the lower and upper rotors, respectively. The second term in Eq. (8) represents the effect of one rotor's wake on the inflow of the other rotor.

In this investigation, the aerodynamic interference needs to be isolated to evaluate the effect of the aerodynamic interference between rotors on the trim characteristics. Thus, during the trim calculation, the second term in Eq. (7) and Eq. (8) can be set to zero to reflect the trim characteristics without the interference between rotors. The basic procedure of the MVRE model in the trim process is shown in Fig. 4. Dashed line denotes the aerodynamic interference between rotors, which is also shown in Eqns (7, 8).

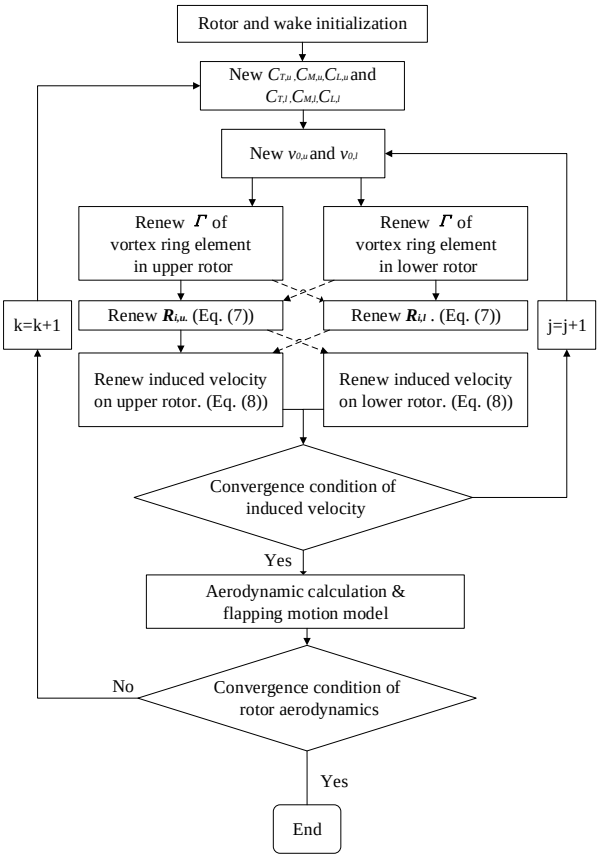

Fig. 4 Trim process of the MVRE model in a coaxial rigid rotor helicopter

2.3 MVRE Model Validation

In this paper, a wind tunnel experiment of the coaxial rotor is utilized to test the precision of the proposed aerodynamic interference model in hover and forward flight states [30]. Moreover, the results of the classic VRE model are used as the basis of comparison to illustrate the improvement of the MVRE model proposed in this article. The basic parameters of the coaxial rotors in the experimental system are demonstrated in Table 1. The advancing ratios of the wind tunnel experiment are $\mu = 0$ (Hover) and $\mu = 0.15$ (forward flight). The torques of the upper and lower rotors maintain balance throughout this

test according to the requirement of the wind tunnel experiment.

Table 1. Parameters of the coaxial rotor in the aerodynamic experiment

Parameter	Value
Rotor radius/m	1.25
Rotor spacing/m	0.2625
Rotor speed/(r/min)	600.0
Number of blades	2×2
Solidity	0.046
Airfoil	NACA23012

Fig. 5 shows the lift coefficient C_T and the torque coefficient m_k results of the MVRE and VRE aerodynamic interference model and the wind tunnel experiment. The results of the MVRE model are consistent with experimental data in the hover and forward flight states. Moreover, the findings indicate that the VRE model has less precision, especially in the hover state, because of the exclusion of extend-retract motion. The proposed MVRE model, in effect, represents the complex interference between the coaxial rotors with precision and can be used to model the flight dynamics characteristics.

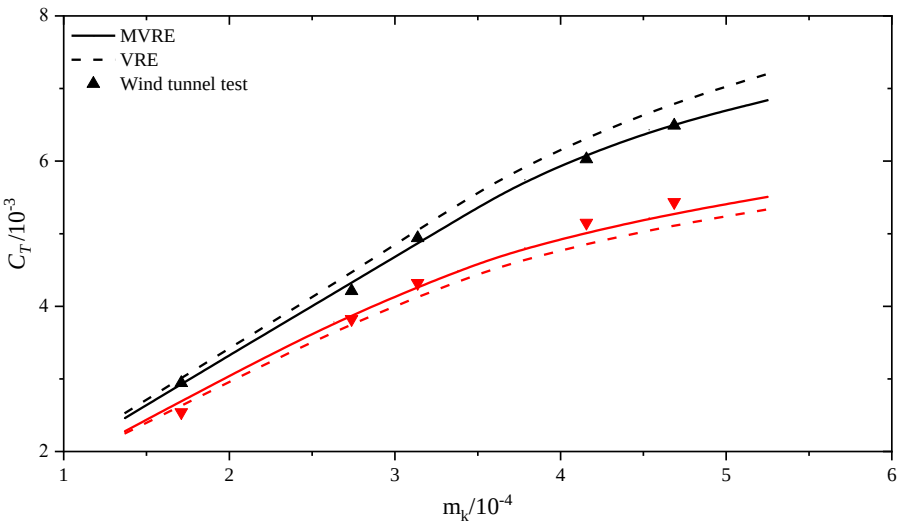

(a) Hover ($\mu = 0$)

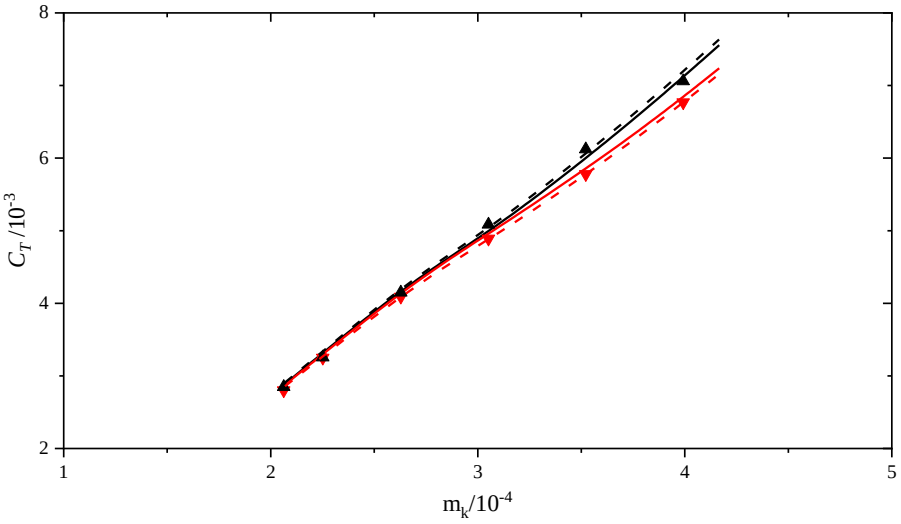

(b) Forward flight ($\mu = 0.15$)

Fig. 5 Coaxial rotor MVRE model comparison results

(the black and red lines represent the upper and lower rotor respectively)

3. Helicopter Flight Dynamics Model

In developing a coaxial rigid rotor helicopter flight dynamics model, the external forces and moments are composed of four parts: rotor, horizontal tail, vertical tail, and fuselage.

3.1 Rotor

In addition to the MVRE model, the coaxial rotor model contains two other parts: the flapping equation and the aerodynamics calculation. The relationship between these parts is shown in Fig. 6.

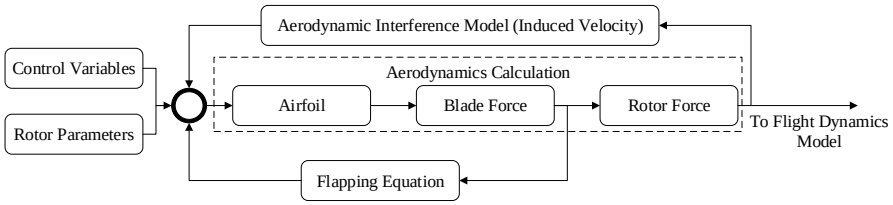

Fig. 6 Coaxial rigid rotor aerodynamics model

The motion of the blade includes the flapping motion and the lead-lag motion. In this article, only the flapping motion is taken into consideration. Because the flapping rigidity of this rotor is significantly higher than that of the conventional rotor and the Coriolis force provided by the flapping motion is lower, the amplitude of the lead-lag motion is relatively small. Therefore, the presence of lead-lag motion contributes little to the overall flight dynamics characteristics of the coaxial rigid rotor helicopter.

The higher flapping rigidity of this rotor also modifies the flight dynamics characteristics of the coaxial rigid rotor helicopter. To simulate the flapping motion more precisely, this paper utilizes the equivalent flapping offset and flapping spring method [31~32]. This equivalent method is shown in Fig. 7.

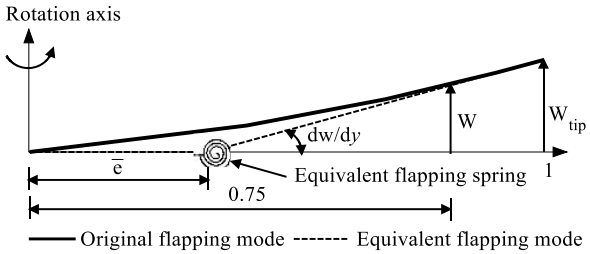

Fig. 7 Rigid blade flapping equivalence

The non-dimensional equivalent flapping offset $\bar{e}$ can be obtained as follows:

$$\bar{e} = 1 - \frac{W_{tip}}{R \cdot W'_{0.75}} \tag{9}$$

where W_{tip} is flapping amplitude at the blade tip; $W'_{0.75}$ is the flapping angle at 0.75R. The equivalent flapping offset is used to fit the blade flapping mode. The rigidity of the equivalent flapping spring given by Eq. (10) is used to guarantee the flapping frequency:

$$K_\beta = (\bar{\omega}_n^2 - 1 - \frac{\bar{e} R M_\beta}{I_\beta}) I_\beta \Omega^2 \tag{10}$$

According to the equivalent method, the flapping motion equation is represented by Eq. (11).

$$\ddot{\beta} + (1 + \bar{e} R M_\beta / I_\beta)\beta + K_\beta \beta / I_\beta \Omega^2 + M_A = 0 \tag{11}$$

where M_A represents the aerodynamic, Coriolis, inertia and gravity moments.

The aerodynamic load calculation, including the airfoil aerodynamics, blade force, and rotor force calculation parts, is similar to that of a conventional rotor [31, 33]. The airfoil section is simulated using the lifting line model based on the airfoil aerodynamics look-up table, and by integrating the results, the aerodynamics of the rotor can be obtained.

3.2 Modelling of Other Parts

Horizontal and Vertical Tails

In this article, the aerodynamic interference of the rotors' wake on tails is taken into consideration through the MVRE model. Eq. (8) can be used to calculate the coaxial rotor wake interference on the horizontal and vertical tails.

In the modelling process of the horizontal and vertical tails, the tails are longitudinally divided into a number of elements with equal area, with every element maintaining the shape of the airfoil. The local velocity vector of each airfoil element can be expressed as follows:

$$\boldsymbol{v}_t = \boldsymbol{v}_\infty + \sum_{j=1,N} \sum_{i=1,M} \boldsymbol{f}(p_{i,j,U}, \gamma_{p_{i,j},U}, P_t) + \sum_{j=1,N} \sum_{i=1,M} \boldsymbol{f}(p_{i,j,L}, \gamma_{p_{i,j},L}, P_t) \tag{12}$$

where P_t represents the position of the element on the tails. Then, the lift and drag coefficients of each airfoil element can be obtained from a 2-D airfoil aerodynamics look-up table with this velocity vector, and the tails' aerodynamics can be calculated by the integration of the aerodynamics at every element

The second and third terms in Eq. (12) represent the effect of the rotor wake on the aerodynamics of tails. When this effect needs to be isolated, these terms are set to zero.

Fuselage

The rotor wake effect on the fuselage aerodynamics can be calculated through the MVRE model.

The velocity on the fuselage reference point is obtained with the consideration of the rotor wake effect as follows:

$$\boldsymbol{v}_f = \boldsymbol{v}_\infty + \sum_{j=1,N}\sum_{i=1,M} \boldsymbol{f}(p_{i,j,U}, \gamma_{p_{i,j},U}, P_f) + \sum_{j=1,N}\sum_{i=1,M} \boldsymbol{f}(p_{i,j,L}, \gamma_{p_{i,j},L}, P_f) \tag{13}$$

where P_f is the reference point of the fuselage. Thus, the attack and sideslip angle of the fuselage can be determined. When these angles are relatively small, the wind tunnel test of the XH-59A helicopter [34] is used to calculate its force and moment coefficients. When the angles are quite large (e.g., the downwash effect in the hover state), a dataset of force and moment coefficients [31] can be used to determine its aerodynamics. These values have been found to reflect the characteristics of a wide range of fuselage shapes when the attack or sideslip angle is relatively large [35].

Similar to the tail model, the latter two terms in Eq. (13) are set to zero when the wake effect on the fuselage needs to be isolated during the investigation.

3.3 Trim Strategy

In the trim process, the helicopter should maintain zero translational and angular acceleration acting at the helicopter's centre of gravity. Therefore, the objective function in this process can be expressed as follows:

$$\begin{bmatrix} X \\ Y \\ Z \end{bmatrix} = \begin{bmatrix} M_{SUM} g \sin\theta \\ -M_{SUM} g \cos\theta \sin\phi \\ -M_{SUM} g \cos\theta \cos\phi \end{bmatrix} \tag{14}$$

$$\begin{bmatrix} L \\ M \\ N \end{bmatrix} = \begin{bmatrix} 0 \\ 0 \\ 0 \end{bmatrix} \tag{15}$$

Conventional helicopters have six trim variables (collective pitch θ_0, longitudinal cyclic pitch θ_{1c}, lateral cyclic pitch θ_{1s}, collective differential θ_{012}, pitching attitude θ, and rolling attitude φ) and the six trim equations (i.e., Eqns. (14~15)) to constitute the trim strategy. However, the trim strategy of the lift-offset (LOS) could be a critical problem in determining the flight dynamics characteristics of the coaxial rigid rotor helicopters [36].

The LOS of the coaxial rigid rotor has a marked impact on its efficiency [37~40]. As LOS is adopted, the lift-centre moves towards the advancing side and the retreating side is offloaded. Therefore, the stall problems can be prevented and the advancing side can reach its maximum lift-drag ratio, thereby improving the rotor efficiency in high-speed flight. LOS can be regulated by the rotor control phase angle Γ_c, which is set to fit the requirement of related flight tests as follows [25]:

$$\Gamma_c = \begin{cases} 40^\circ, V_f < 40 \text{ m/s} \\ 50^\circ, 50\text{m/s} \geq V_f \geq 40 \text{ m/s} \\ 60^\circ, V_f > 50 \text{ m/s} \end{cases} \tag{16}$$

4. Trim Investigation

4.1 Validation in Trim Results

The example coaxial rigid rotor helicopter in this paper is the XH-59A helicopter. The basic parameters of the XH-59A are shown in Table 2 [25, 41].

Table 2. XH-59A helicopter parameters

Parameter	Value
Rotor radius/m	5.49

Number of blades	3×2
Pre-twist/(°)	-10
Rotor speed/(rad/s)	35.9
Taper ratio	0.5
Flapping frequency/Ω	1.4
Shaft spacing/m	0.77
Horizontal tail area/m^2	5.57
Vertical tail area/m^2	2.79
Take-off weight/kg	5500
Lower rotor position/m	(0.00,0.00,-0.89)
Centre of gravity/m	(0.00,0.00,0.00)
Horizontal tail position/m	(-6.80,0.00,0.20)
Vertical tail position/m	(-6.80,0.00,-0.50)

In the trim validation process, the trim results with the flight dynamics model on the basis of the MVRE aerodynamic interference model are shown in Fig. 8 from hover (0 m/s) to 80 m/s. The trim results of the XH-59A rotorcraft flight test data [25] are added for comparison.

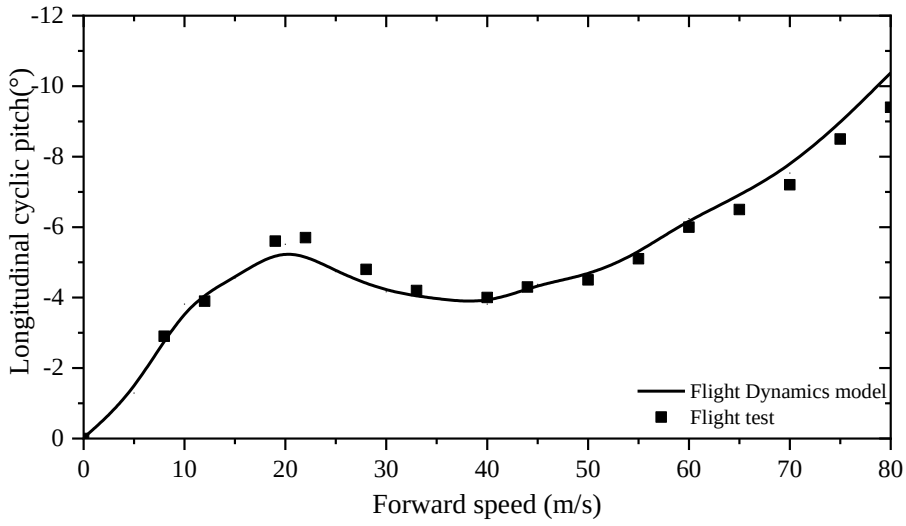

(a) Longitudinal cyclic pitch

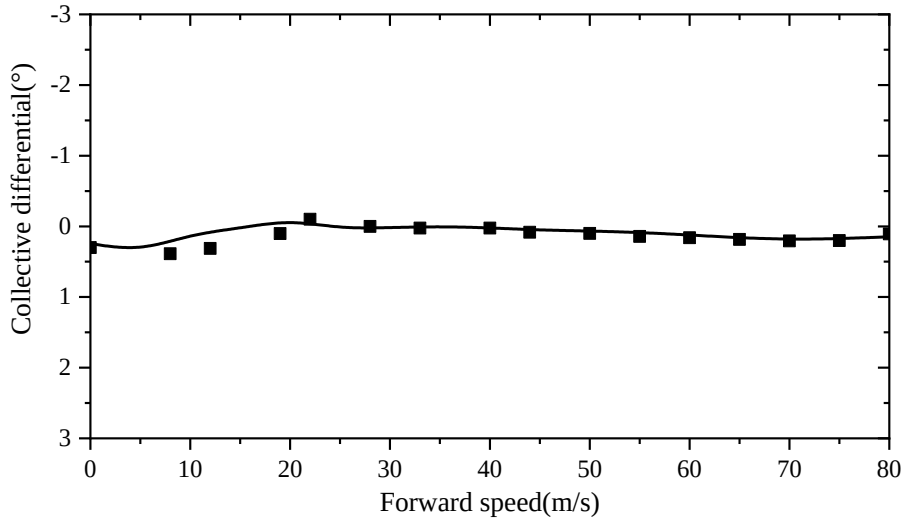

(b) Collective differential

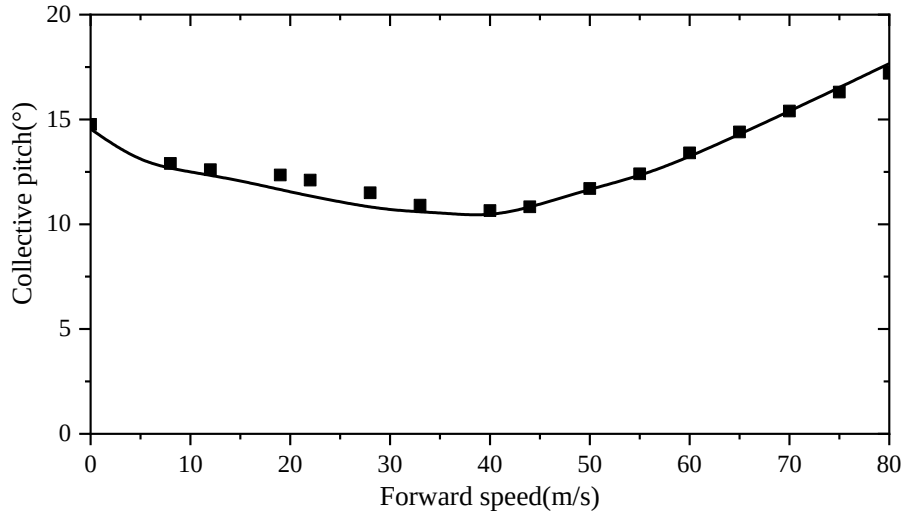

(c) Collective pitch

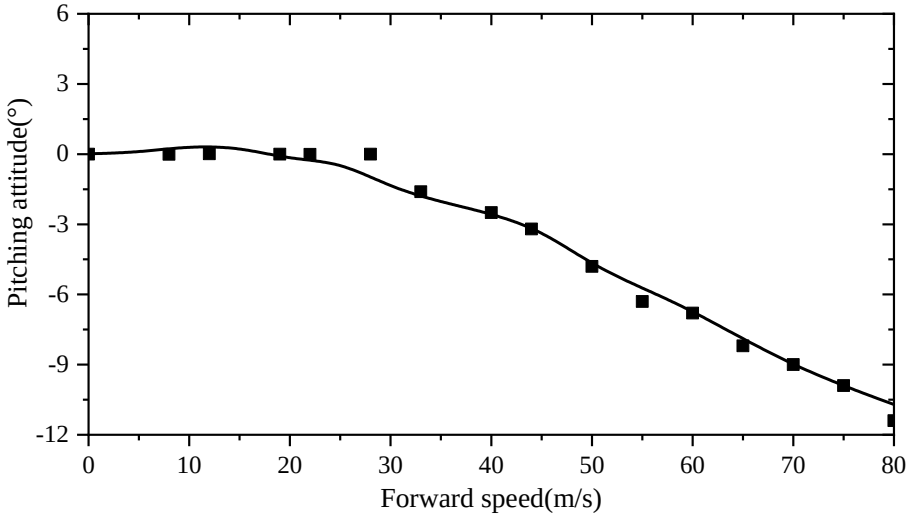

(d) Pitching attitude

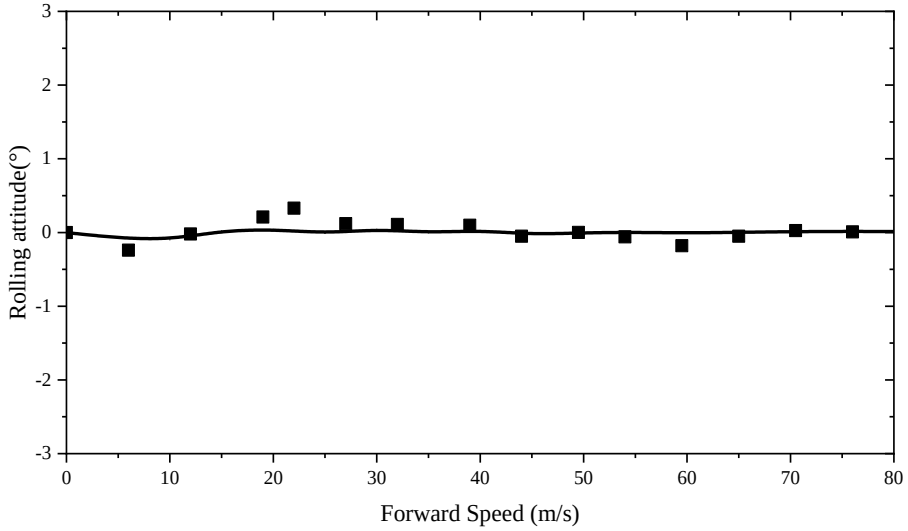

(e) Rolling Attitude

Fig. 8 Trim results

The comparison results suggest that the proposed flight dynamics model with consideration of all aerodynamic interference can be used to accurately simulate the trim characteristics of coaxial rigid rotor helicopters. Fig. 9 shows the trim computing time using the flight dynamics model based on the MVRE model and the free-wake model [20, 21]. With the same computing environment (CPU: i7-4700; Memory: 16GB; without parallelization), the results indicate that the computing time of MVRE model (100 s ~ 200 s) is relatively lower compared to that of the free-wake method (1400 s ~ 2000 s).

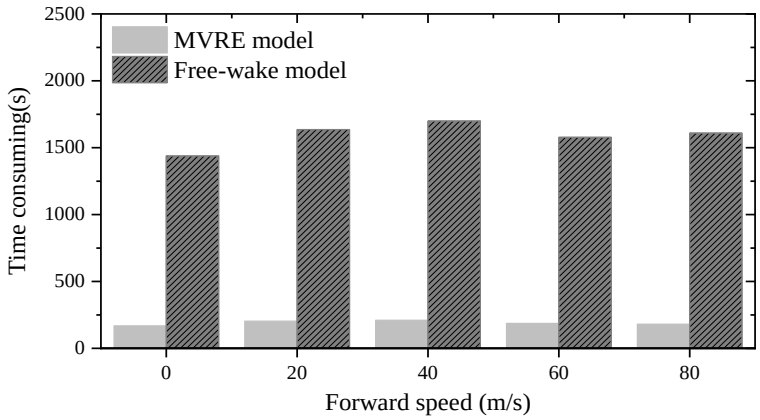

Fig. 9 Computing time comparison

4.2 Aerodynamic Interference on Trim Characteristics

Aerodynamic interference of the coaxial rigid rotor helicopter can be divided into three parts: the aerodynamic interference between rotors, the interference of the rotor wake on the horizontal and vertical tails, and the interference of rotor wake on the fuselage. The MVRE model facilitates the investigation of these effects on the trim characteristics.

Aerodynamic Interference between Rotors

Based on the illustration in section 2.3, the coaxial rotor's aerodynamic interference effect on the trim characteristics can be easily isolated. Fig. 10 shows the trim results of the coaxial rigid rotor helicopter with and without considering the aerodynamic interference between coaxial rotors, with the flight data results shown for comparison.

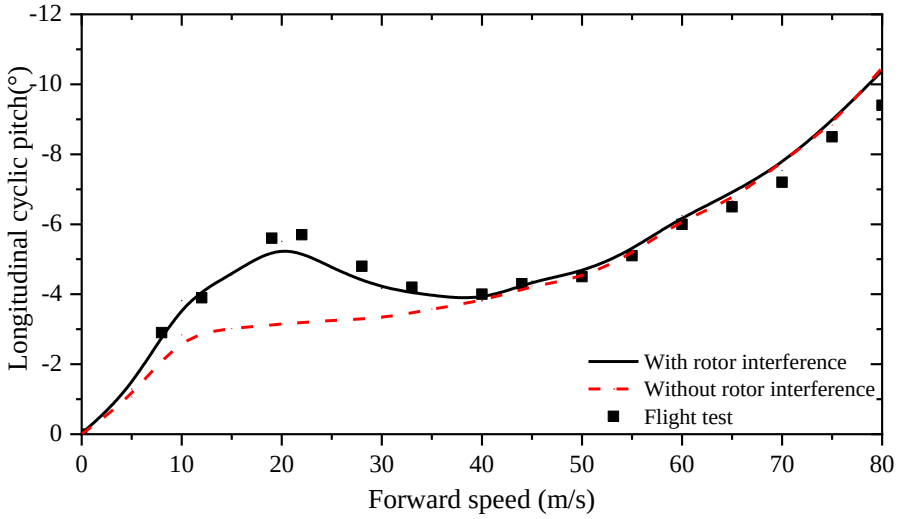

(a) Longitudinal cyclic pitch

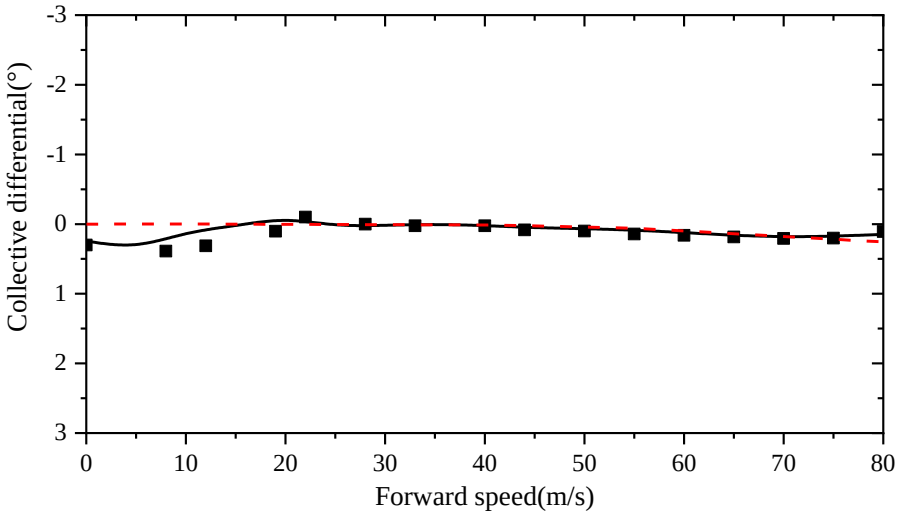

(b) Collective differential

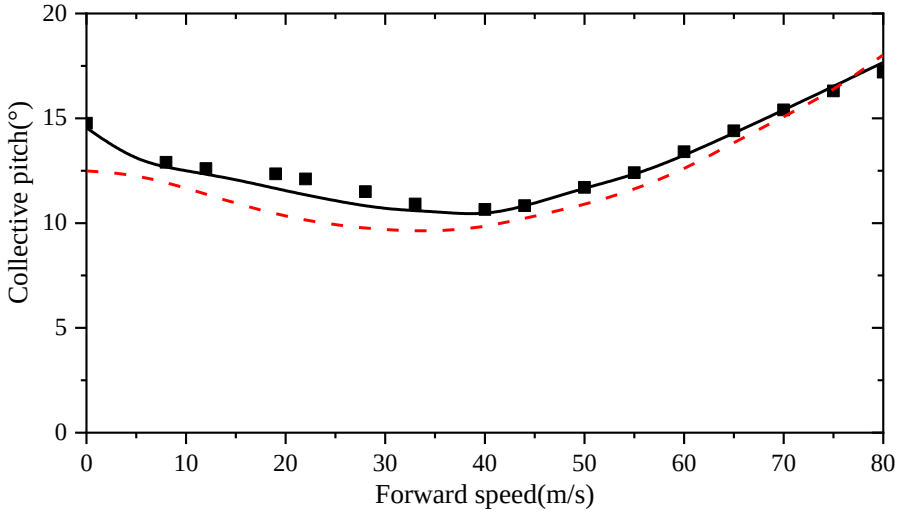

(c) Collective pitch

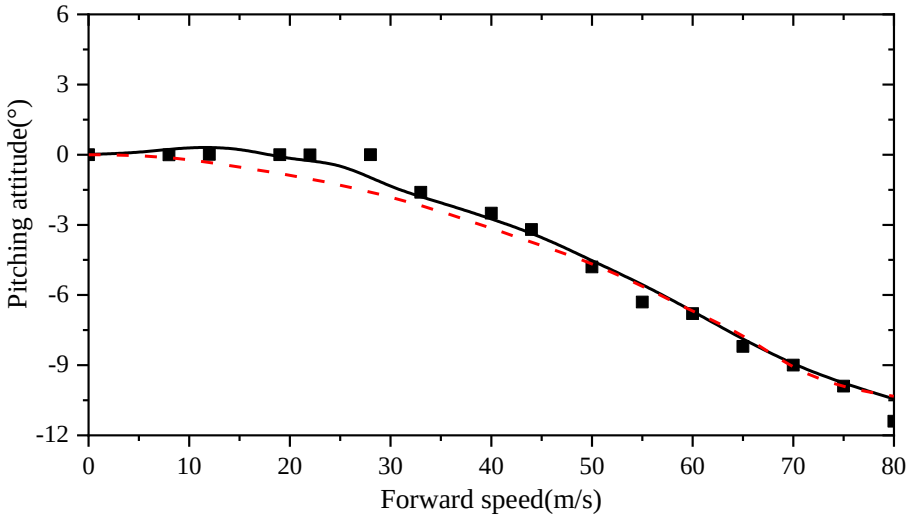

(d) Pitching attitude

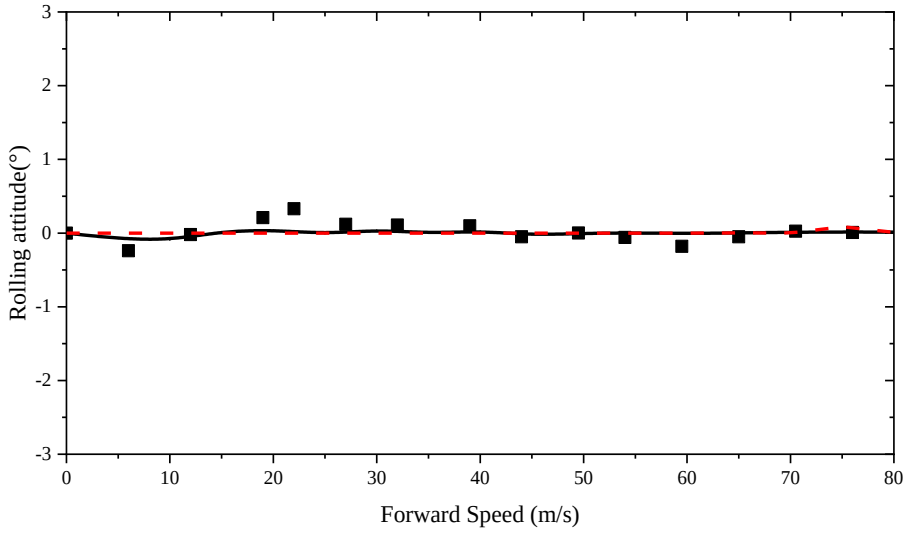

(e) Rolling Attitude

Fig. 10 Aerodynamic interference effect between rotors on the trim results

According to the comparison, the aerodynamic interference between rotors has an influence on the trim characteristics of the coaxial rigid rotor helicopter. The wake shapes calculated by the MVRE model with various forward speeds are also obtained to illustrate the effect of interference between rotors on the trim characteristics, as shown in Fig. 11.

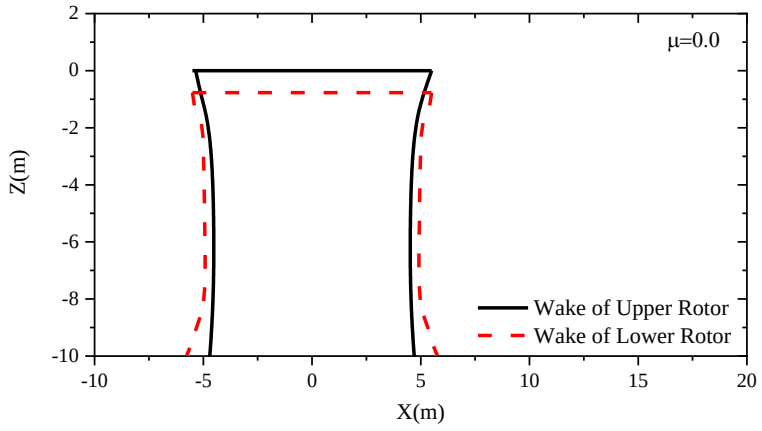

(a) Hover

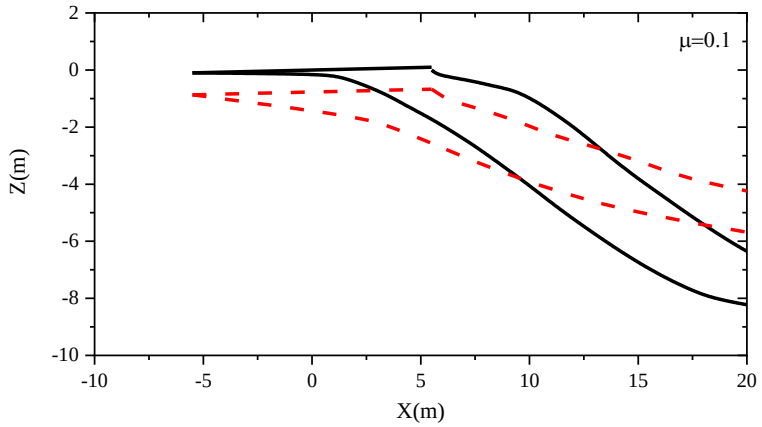

(b) 20 m/s

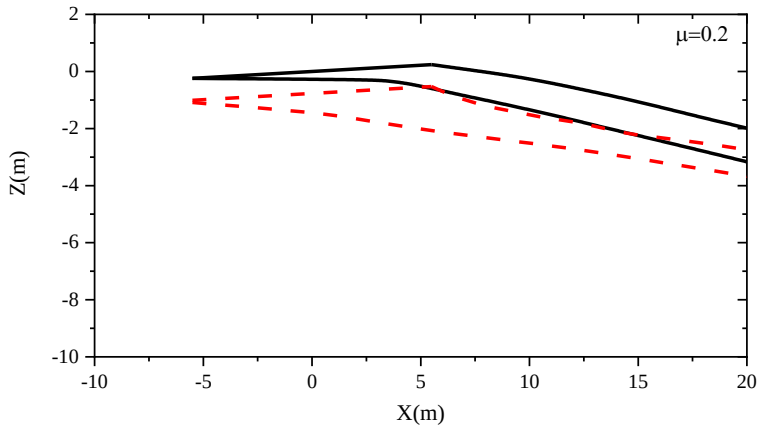

(c) 40 m/s

Fig. 11 Wake shape of the coaxial rotor at different forward speeds

According to Fig. 10 and Fig. 11, the influence of coaxial rotor interference on the collective pitch and collective differential is similar to those of other conventional helicopters [13]. The interference between rotors increases the collective pitch during trim flight and is more evident in hover and low-speed forward flight. In this speed range, aerodynamic interference between rotors increases the inflow of the lower rotor and consequently reduces the thrust of coaxial rotor at a given collective pitch; as a result, the pilot must input more collective pitch to balance the vehicle. Moreover, the increment of the inflow in the lower rotor requires more collective differential to maintain torque balanced. In high-speed forward flight, the aerodynamic interference effect decreases; thus, the collective differential is reduced to approximately zero and the collective pitch results with and without considering aerodynamic interference become similar.

In addition, coaxial rigid rotor helicopters have unique aerodynamic interference feature, which is the trim characteristics in the longitudinal cyclic pitch and the pitching attitude. The influence is most significant in low-speed forward flight, at which the interference causes the longitudinal cyclic pitch to have a negative gradient under forward speed and also leads the pitch attitude to be slightly higher.

This influence is caused by both the interference effect and the features of the rigid rotor. To analyse this effect, the contour figures of the induced velocities on the upper and lower rotors are shown in Fig. 12 at hover, 20 m/s, and 40 m/s.

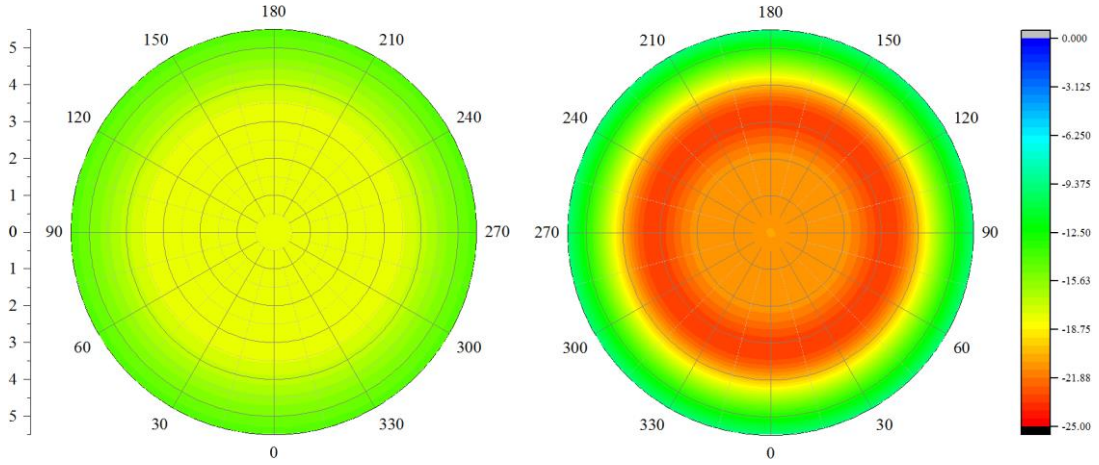

(a) Hover, $\mu = 0$

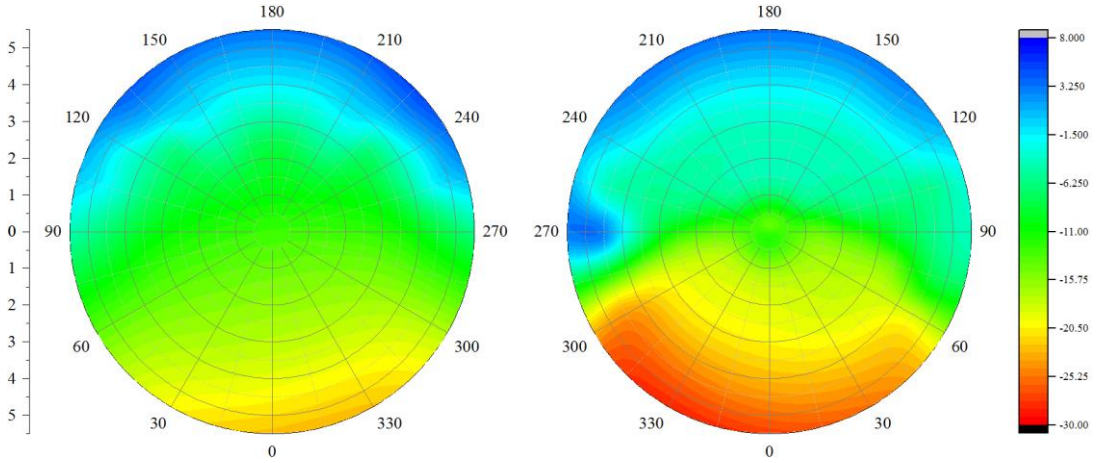

(b) $V = 20m/s, \mu = 0.1$

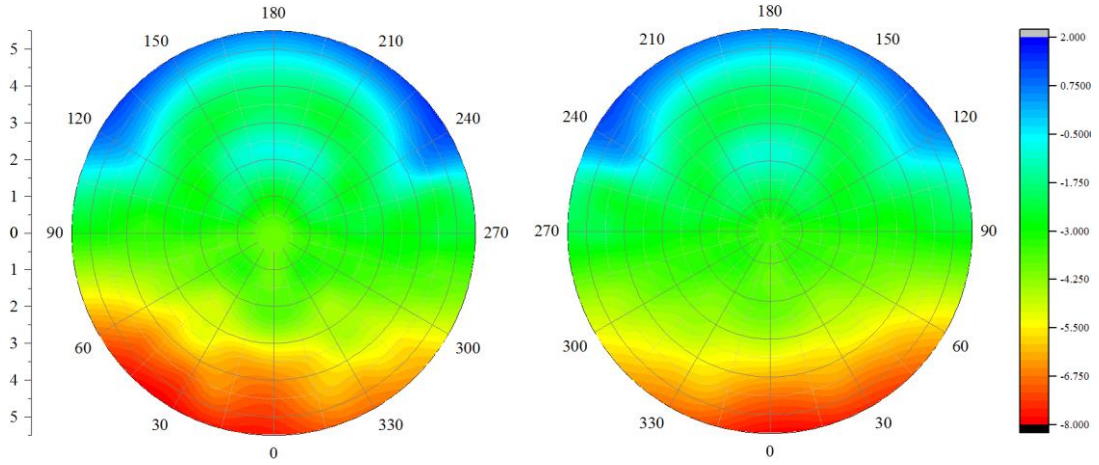

(c) $V = 40m/s, \mu = 0.2$

Fig. 12 Contour figures of the induced velocity on the upper and lower rotor (lower rotor on the right)

According to Fig. 12, the wake of the upper rotor mainly affects the backside of the lower rotor when the advancing ratio is 0.1 (20 m/s forward flight), and it causes extra downwash velocity in this area. In other words, the inflow of the rear part on the lower rotor becomes larger. On the other hand, the flapping frequency of the coaxial rigid rotor is much higher than that of conventional helicopters, thus causing a change in the phase difference between the azimuth angle of additional inflow and the direction of the hub moment it induced. This phase difference is called the flapping response lag angle ϕ, which is

dependent on the flapping frequency and given as follows [31]:

$$\cos\phi = \frac{\left(\bar{\omega}_n^2 - 1\right)^2}{\sqrt{\left(\bar{\omega}_n^2 - 1\right)^2 + 4\xi^2\bar{\omega}_n^2}} \tag{17}$$

where ξ is the damping ratio, which is usually around 0.5. The flapping frequency of the coaxial rigid rotor is close to 1.4, and ϕ is approximately 30 degrees according to Eq. (17). Therefore, the interference inflow of the lower rotor would mainly add the pitching moment to the vehicle, which requires the pilot to input more longitudinal cyclic pitch to maintain the trim state. When the helicopter is in hover, the interference on the lower rotor is symmetrical and cannot lead to additional pitching hub moment. With the forward speed increases, the rear part of the lower rotor is affected by the rotor wake of the upper rotor, which induces the upward pitching moment and needs additional longitudinal cyclic pitch to balance it. Next, as further increases the forward speed, the aerodynamic interference is no longer significant and the effect on the trim result becomes diminished. The input of the longitudinal cyclic pitch is reduced at this flight range. Therefore, the aerodynamic interference between rotors causes a negative gradient phenomenon on the longitudinal cyclic pitch results.

The pitching attitude is also influenced due to the aerodynamic interference between coaxial rotors. As analysed above, this interference increases the longitudinal cyclic pitch, causing the tip path plane to tilt forward, which results in more forward force to the helicopter. Thus, the vehicle should be tilted backward to maintain the balance in the forward force. The change in pitching attitude is usually in accordance with the change in the tip path plane angle. However, the increment of tip path plane angle is much less than the increment of longitudinal cyclic pitch due to the higher flapping frequency [42]. The interference induced alteration in pitching attitude is consequently much lower than that in the longitudinal cyclic pitch.

Rotor Wake Influence on Other Parts

The MVRE model facilitates the consideration of the rotor wake effect on the horizontal tail, vertical tail, and the fuselage. The modelling process of these effects was illustrated above. The various types of influence can be isolated by executing the trim process without the related parts (the latter two terms in Eqns. (12~13)). Therefore, the aerodynamic interference of the rotor-horizontal tail (rotor-HT), rotor-fuselage (rotor-FU), and rotor-vertical tail (rotor-VT) on the trim characteristics is obtained as shown in Fig. 13.

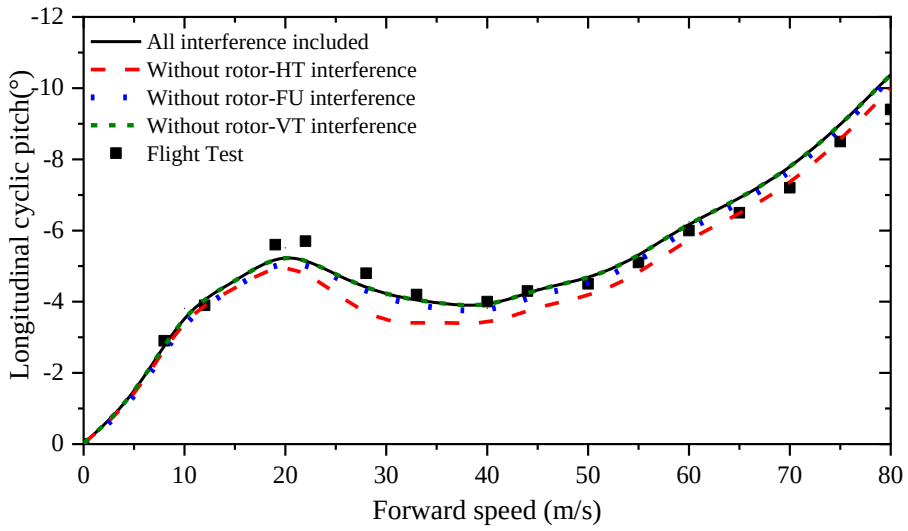

(a) Longitudinal cyclic pitch

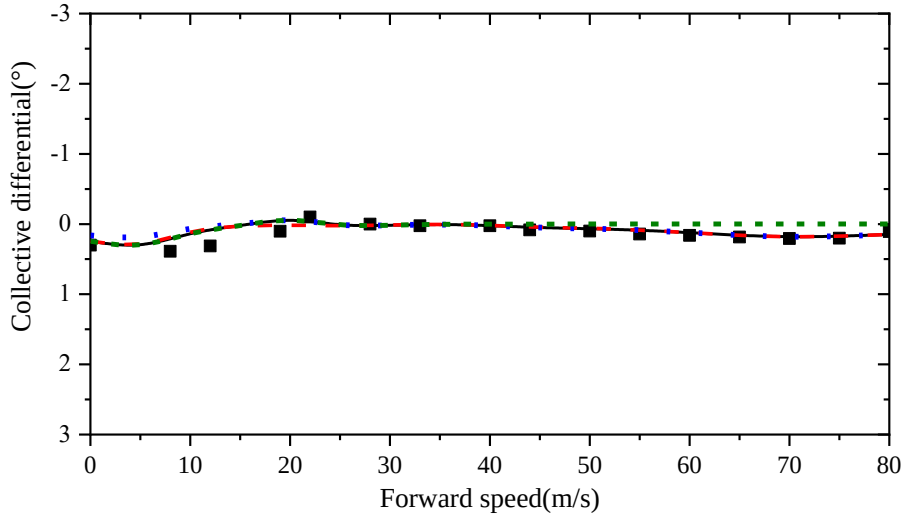

(b) Collective differential

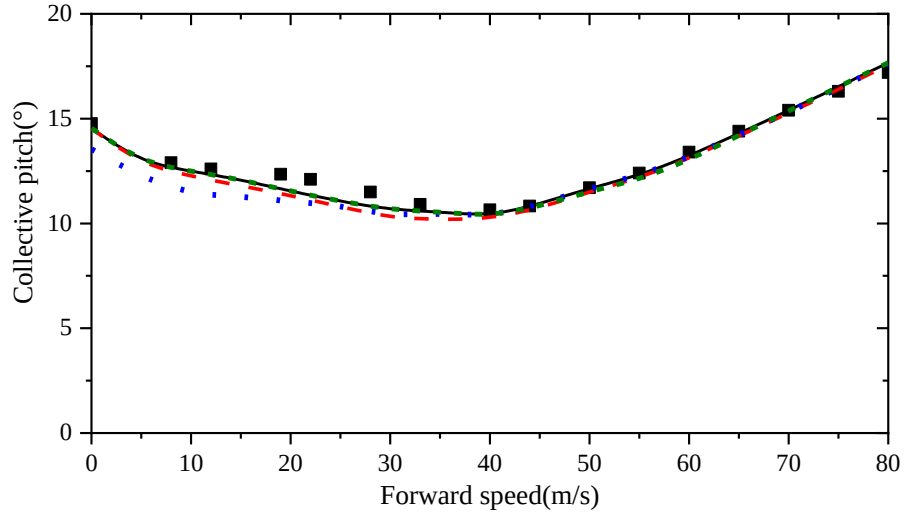

(c) Collective pitch

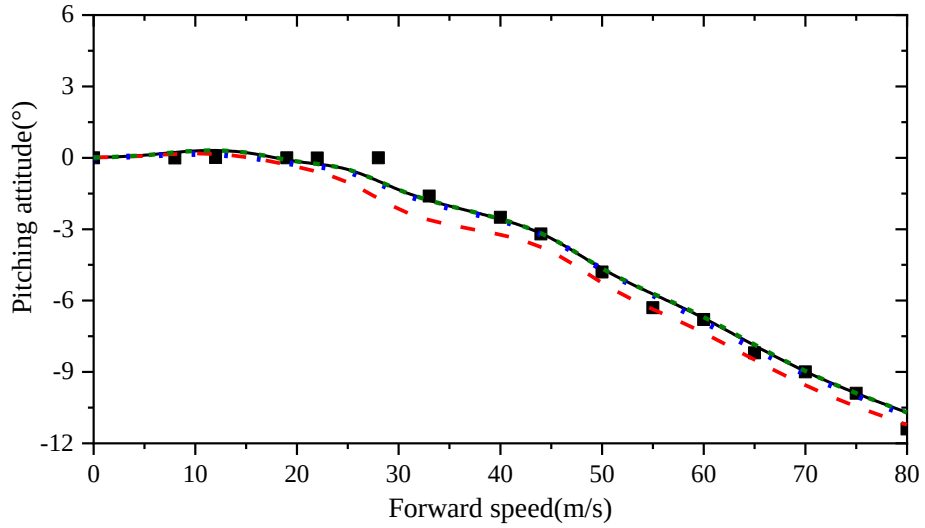

(d) Pitching attitude

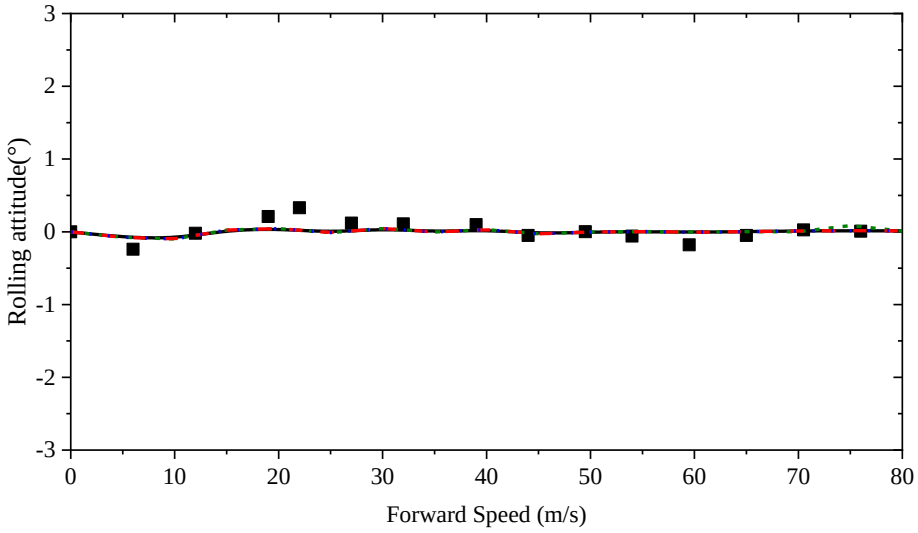

(e) Rolling attitude

Fig. 13 Rotor wake-other parts interference effect on the trim results

The rotor wake interference on the horizontal tail alters the longitudinal cyclic pitch and pitching attitude trim results. The horizontal tail is situated in the wake at the mid speed flight range, thereby producing extra upward moment. This phenomenon would also occur for the conventional helicopters. However, the amplitude of this influence in the coaxial rigid rotor helicopter is much lower than other helicopters [43] because the higher flapping frequency increases the control power of the longitudinal cyclic pitch. The longitudinal cyclic pitch control derivative can be expressed as Eq. (18) based on the flapping equation [42]:

$$\frac{\partial M}{\partial \theta_{1c}} = -N_b \frac{K_\beta}{2}\left[\frac{16\gamma_c(\bar{\omega}_n^{\,2}-1)(\mu^2+2)}{256(\bar{\omega}_n^{\,2}-1)^2+\gamma_c^{\,2}(4-\mu^4)}\cos(\Gamma_c)+\frac{\gamma_c^{\,2}(4-\mu^4)}{256(\bar{\omega}_n^{\,2}-1)^2+\gamma_c^{\,2}(4-\mu^4)}\sin(\Gamma_c)\right] \quad (18)$$

The increments of wake-induced pitching moment on the horizontal tail for various helicopters are more similar; however, the control derivative of the longitudinal cyclic pitch in coaxial rigid rotor helicopter is much higher according to Eq. (18). In other words, the longitudinal cyclic pitch could provide a higher pitching moment with relatively less control input. Therefore, the effect of wake-horizontal tail interference on the longitudinal cyclic pitch is much lower (the maximum effect is 0.7 degrees at the speed of approximately 30 m/s).

The rotor wake interference on the vertical tail has only a minor influence on the trim results. This influence is relatively more evident in the collective differential and rolling attitude because the aerodynamic interference increases the attack angle of the vertical tail slightly and adds a yawing moment and sideward force.

The rotor wake influence on the fuselage mainly affects the collective pitch in hover and low-speed forward flight. The fuselage is partly situated in the wake of the coaxial rotors; thus, the interference from the rotors adds negative lift, which is similar to the conventional helicopter.

5. Conclusions

A flight dynamics model of the coaxial compound helicopter based on the MVRE aerodynamic interference model was established. The precision levels of the MVRE model and associated flight dynamics model were evaluated through wind tunnel and flight test data. Moreover, the various types of aerodynamic interference can be isolated using the MVRE model so that these effects can be individually analysed. Our conclusions are given as follows.

1. The flight dynamics model associated with the MVRE model has satisfactory accuracy to consider the effect of aerodynamic interference on the trim characteristics. In addition, the computing efficiency of the MVRE model is considerably improved.
2. According to trim characteristics, the aerodynamic interference between rotors not only influences the collective pitch and collective differential trim results (such as that in a conventional coaxial helicopter), but also changes the longitudinal cyclic pitch and the pitching attitude because of the higher flapping frequency of the coaxial rigid rotor.
3. The influence of the rotor wake on the horizontal tail would change the longitudinal cyclic pitch and pitching attitude trim results. However, this influence is less than that of other conventional helicopters because of the higher control power in the longitudinal cyclic pitch. Moreover, the effect of the rotor wake on the fuselage adds the collective pitch during hover and low-speed flight, and the rolling attitude and collective differential results are slightly affected during high-speed flight due to the rotor wake influence on the vertical tail.

References:

1. Ferguson, Kevin, Douglas Thomson. Flight dynamics investigation of compound helicopter configurations. J AIRCRAFT. 52(1) (2014) 156-167.
2. Yeo, Hyeonsoo, and Wayne Johnson. Optimum design of a compound helicopter. J AIRCRAFT. 46(4) (2009) 1210-1221.
3. Darrow DA, Bertolotti FP, Sbabo TL, D'anna FP, inventors; Sikorsky Aircraft Corp, assignee. De-rotation system for a counter-rotating, coaxial rotor hub shaft fairing. United States patent US 7,621,480. 2009 Nov 24.
4. Kim, H.W. and Kenyon, A.R. and Duraisamy, K. and Brown, R.E. (2008) Interactional aerodynamics and acoustics of a propeller-augmented compound coaxial helicopter. In: 9th American Helicopter Society Aeromechanics Specialists' Meeting, 23-25 January 2008, San Francisco, California.
5. Feil, Roland, Juergen Rauleder, and Manfred Hajek. Aeromechanics Analysis of a Coaxial Rotor System in Hover and High-Advance-Ratio Forward Flight. 34th AIAA Applied Aerodynamics Conference, AIAA. 2016.
6. Passe, Bradley J., Ananth Sridharan, and James D. Baeder. Computational investigation of coaxial rotor interactional aerodynamics in steady forward flight. 33rd AIAA Applied Aerodynamics Conference, AIAA, 2015.
7. Schmaus, Joseph Henry. Aeromechanics of a High Speed Coaxial Helicopter Rotor. Diss. University of Maryland, College Park, 2017.
8. Ferguson, Kevin, and Douglas Thomson. Performance comparison between a conventional helicopter and compound helicopter configurations. P I MECH ENG G-J AER 229 (13) (2015) 2441-2456.
9. Enconniere, Julien, Jesus Ortiz-Carretero, and Vassilios Pachidis. Mission performance analysis of a conceptual coaxial rotorcraft for air taxi applications. AEROSP SCI TECHNOL 69 (2017) 1-14.
10. Leishman, J. Gordon, and Shreyas Ananthan. An optimum coaxial rotor system for axial flight. J AM HELICOPTER SOC 53(4) (2008) 366-381.
11. Leishman, J. Gordon, and Monica Syal. Figure of merit definition for coaxial rotors. J AM HELICOPTER SOC 53(3) (2008) 290-300.
12. Syal, Monica, and J. Gordon Leishman. Aerodynamic optimization study of a coaxial rotor in hovering flight. J AM HELICOPTER SOC 57(4) (2012) 1-15.
13. Heyong, X. U., and Y. E. Zhengyin. Numerical simulation of unsteady flow around forward flight helicopter with coaxial rotors. CHINESE J AERONAUT 24(1) (2011): 1-7.
14. Lakshminarayan, Vinod K., and James D. Baeder. Computational investigation of microscale coaxial-rotor

aerodynamics in hover. J AIRCRAFT 47(3) (2010): 940-955.

15. Anusonti-Inthra, Phuriwat. Full Vehicle Simulations for a Coaxial Rotorcraft Using High-Fidelity CFD/CSD Coupling. 2018 AIAA Aerospace Sciences Meeting. AIAA.2018.

16. Zhao, Jinggen and He, Chengjian Real-Time Simulation of Coaxial Rotor Configurations with Combined Finite State Dynamic Wake and VPM. American Helicopter Society 70th Annual Forum, Montreal Canada. American helicopter society, INC. May 20-22, 2014

17. Zhao, Jinggen, and Chengjian He. A Finite State Dynamic Wake Model Enhanced with Vortex Particle Method–Derived Modeling Parameters for Coaxial Rotor Simulation and Analysis. J AM HELICOPTER SOC 61(2) (2016) 1-9.

18. Schmaus, Joseph H., and Inderjit Chopra. Aeromechanics of rigid coaxial rotor models for wind-tunnel testing. J AIRCRAFT 54(4) (2017) 1486-1497.

19. Lyu, Wei-Liang, and Guo-Hua Xu. New-Trim-Method-Based Investigation on the Cyclic-Pitch-Effected Advancing-Blade-Concept Helicopter Aerodynamics. J AIRCRAFT 52 (4) (2015) 1365-1371.

20. Li, Pan, and Renliang Chen. Rotor unsteady aerodynamics model using an efficient free-vortex method. AIRCR ENG AEROSP TEC 84(5) (2012) 311-320.

21. Xin, Ji, Renliang Chen, and Pan Li. Time-stepping free-wake methodology for rotor flow field simulation in ground effect. AIRCR ENG AEROSP TEC 87(5) (2015): 418-426.

22. Basset P M. Modeling of the dynamic inflow on the main rotor and the tail components in helicopter flight mechanics. 22nd European Rotorcraft Forum, Brighton, UK. ERF. 1996:104.

23. Basset P M, Tchen-Fo F. Study of the rotor wake distortion effects on the helicopter pitch-roll Cross-couplings. European Rotorcraft Forum. Associazione Italiana di Aeronautica ed Astronautica, ERF. 1998.

24. Basset, P M., and R. A. Ormiston. Comparison and validation of the France/USA finite state rotor dynamic inflow models. 36th European Rotorcraft Forum, Paris, France. ERF. September 7-9, 2010.

25. Ruddell, A. J., W. Groth, and R. McCutcheon. Advancing blade concept (ABC) technology demonstrator. No. SER-69065. United Technologies Corp Stratford Ct Sikorsky Aircraft Div, ADA100181, 1981.

26. Halley D H. ABC helicopter stability, control, and vibration evaluation on the Princeton dynamic model track. American Helicopter Society, Annual National Forum, 29 th, Washington, D. C. American Helicopter Society, Inc. 1973.

27. Johnson, Wayne. Helicopter theory. Courier Corporation, 2012.

28. Vatistas G H. Simple Model for Turbulent Tip Vortices. J AIRCRAFT. 43(5) (2014) 1577-1579.

29. Vatistas, Georgios H., V. Kozel, and W. C. Mih. A simpler model for concentrated vortices. EXP FLUIDS 11(1) (1991): 73-76.

30. Deng Y M, Tao R, Hu J Z. Experimental Investigation of the Aerodynamic Interaction between Upper and Lower Rotors of a Coaxial Helicopter. Acta Aeronautica et Astronautica Sinica, 24(1) (2003) 10-14. (In Chinese)

31. Padfield, Gareth D. Helicopter flight dynamics: the theory and application of flying qualities and simulation modelling. John Wiley & Sons, 2008.

32. Leishman, Gordon J. Principles of helicopter aerodynamics with CD extra. Cambridge university press, 2006.

33. Yuan Y, Chen R L, Li P. Trim characteristics and verification of coaxial rigid rotor aircraft. Journal of Nanjing University of Aeronautics & Astronautics, 48 (2) (2016) 186-193 (In Chinese).

34. Phelps.A E, Mineck R E. Aerodynamic characteristics of a counter-rotating, coaxial, hingeless rotor helicopter model with auxiliary propulsion. NASA-TM-78705, May, 1978.

35. Laxman, Vaitla, et al. Power and trim estimation for helicopter sizing and performance analysis. INT J AERONAUT SPACE 12 (2) (2011) 156-162.

36. Johnson, Wayne, Alex M. Moodie, and Hyeonsoo Yeo. Design and performance of lift-offset rotorcraft for short-haul missions. National Aeronautics and Space Administration Moffett Field Ca Ames Research Center, ADA563404, 2012.

37. Kim, Hyo Wan, Karthikeyan Duraisamy, and Richard Brown. Effect of rotor stiffness and lift offset on the aeroacoustics of a coaxial rotor in level flight. 65th American Helicopter Society Annual Forum. AMERICAN HELICOPTER SOCIETY, INC. 2009.

38. Lim, JaeHoon, SangJoon Shin, and YoungJung Kee. Optimization of rotor structural design in compound rotorcraft with lift offset. J AM HELICOPTER SOC 61(1) (2016): 1-14.

39. Bagai, Ashish. Aerodynamic design of the X2 technology demonstrator™ main rotor blade. 64th American Helicopter Society Annual Forum. American Helicopter Society, INC, 2008.

40. Blackwell, R., and T. Millott. Dynamics design characteristics of the Sikorsky X2 technology™ demonstrator aircraft. 64th American Helicopter Society Annual Forum. American Helicopter Society, INC, 2008.

41. Felker III, Fort F. Performance and Loads Data from a Wind Tunnel Test of a Full-Scale, Coaxial, Hingeless Rotor Helicopter. No. NASA-A-8732. National Aeronautics and Space Administration Moffett Field Ca Ames Research Center, ADA110278, 1981.

42. Chen, Robert TN. Effects of primary rotor parameters on flapping dynamics. NASA, NASA-TP-1431. (1980).

43. Laxman, V., and C. Venkatesan. Influence of dynamic stall and dynamic wake effects on helicopter trim and rotor loads. J AM HELICOPTER SOC 54(3) (2009): 32001-32001.